Silicon nitride micromesh bolometer arrays for SPIRE

James J. Bock, Jason Glenn, Sabrina M. Grannan, Kent D. Irwin, Andrew E. Lange, et al.

James J. Bock, Jason Glenn, Sabrina M. Grannan, Kent D. Irwin, Andrew E. Lange, Henry G. LeDuc, A. D. Turner, "Silicon nitride micromesh bolometer arrays for SPIRE," Proc. SPIE 3357, Advanced Technology MMW, Radio, and Terahertz Telescopes, (31 July 1998); doi: 10.1117/12.317365

SPIE.

Event: Astronomical Telescopes and Instrumentation, 1998, Kona, HI, United States

Silicon nitride micromesh bolometer arrays for SPIRE

James J. Bock[a], Jason Glenn[b], Sabrina M. Grannan[a], Kent D. Irwin[c], Andrew E. Lange[b], Henry G. LeDuc[a], and A.D. Turner[a]

[a]Jet Propulsion Laboratory, 4800 Oak Grove Dr., Pasadena, CA 91109
[b]California Institute of Technology, Pasadena, CA 91125
[c]National Institute of Standards and Technology, Boulder CO 80303

ABSTRACT

We are developing arrays of bolometers based on silicon nitride micromesh absorbers for the Spectral & Photometric Imaging Receiver (SPIRE) on the Far Infra-Red and Submillimeter Space Telescope (FIRST). The bolometers are coupled to a close-packed array of 1 $f\lambda$ feedhorns which views the primary mirror through a cooled aperture stop. Feedhorn-coupled bolometers minimize the detector area and throughput and have good optical efficiency. A 1 $f\lambda$ feedhorn array provides higher mapping speed than a $2f\lambda$ feedhorn array and reduces the number of jitters required to produce a fully sampled map, but at the cost of more detectors. Individual silicon nitride micromesh bolometers are already able to meet the performance requirements of SPIRE. In parallel we are developing transition-edge detectors read out by a SQUID current amplifier. The relatively large cooling power available at 300 mK enables the array to be coupled to a cold SQUID multiplexer, creating a monolithic fully multiplexed array and making large format arrays possible for SPIRE.

Keywords: infrared detectors, bolometers, arrays

1. INTRODUCTION

New arrays of high sensitivity bolometers promise to improve the sensitivity of instruments for astrophysics in the relatively unexplored spectral region of the far-infrared and millimeter. These wavelengths are very rich for cosmology and astrophysics, and include both the cosmic microwave background radiation, which has not significantly interacted with matter since it was created when the universe was ionized at $z \sim 1000$, and the recently discovered cosmic far-infrared background radiation[1], which is presumably the integrated light from the first stars that formed in the universe. Anisotropies in the cosmic microwave background, which trace the matter anistotropies at the time of last scattering that seeded the formation of structures we observe in clusters and galaxies today, are a powerful tool for cosmology. The formation of the first galaxies is just beginning to be probed in deep optical surveys. If protogalaxies tend to be dusty, as the amplitude of the recently discovered far-infrared background suggests, their thermal dust emission is redshifted into the far-infrared and millimeter. These wavelengths are also ideal to detect the early stages of star formation from cold condensations in molecular clouds, and the kinetic Sunyaev-Zel'dovich effect in clusters. The SPIRE instrument on FIRST (see Griffin *et al.* in these proceedings) will use arrays of high sensitivity bolometers to search for the emission from the first population of galaxies and for studies of star formation.

SPIRE has an imaging photometer which simultaneously views the sky in three wave-bands nominally centered at 250, 350 and 500 μm with spectral resolution $\delta\lambda/\lambda \sim 3$ (see Griffin *et al.* in these proceedings). In addition, two bolometer arrays coupled to the output of a Martin-Puplett Fourier transform spectrometer with variable resolution 0.04 - 0.2 cm^{-1} will provide flexible imaging spectroscopy from 200 - 670 μm. The requirements on the detectors for the imaging photometers and the FTS are listed in Table 1. Because the primary science goal of SPIRE is to search for dusty protogalaxies, the mapping speed, or the time required to map a region of sky down to a given flux limit, is the most important specification of the instrument to be optimized. Although the speed and sensitivity requirements for SPIRE are within the parameters of existing

Further author information -
J.J.B. (correspondence): Email: James.J.Bock@jpl.nasa.gov; Telephone: (818)-354-0715; Fax: (626)-584-9929
J.G.: jg@astro.caltech.edu; (626)-395-2016; S.M.G.: Sabrina.M.Grannan@jpl.nasa.gov; (818)-354-1744
K.D.I.: inwin@boulder.nist.gov; A.E.L.: ael@astro.caltech.edu; (818)-395-6887
H.G.L.: Henry.G.LeDuc@jpl.nasa.gov; (818)-354-2209; A.D.T.: Anthony.D.Turner@jpl.nasa.gov; (818)-393-4420

Part of the SPIE Conference on Advanced Technology MMW, Radio, and Terahertz Telescopes
Kona, Hawaii • March 1998 SPIE Vol. 3357 • 0277-786X/98/$10.00

bolometers, as discussed below, the ability to read out a large array of low-noise bolometers with low power dissipation on the focal plane does not yet exist. Therefore the development of a cold multiplexer technology and the choice of the architecture of the bolometer arrays are crucial technical issues for SPIRE.

Bolometer technology has progressed rapidly in recent years, with advances in microfabrication enabling large format arrays of bolometers to be a reality for FIRST. Very recent development with transition-edge superconductor (TES) bolometers coupled to a SQUID multiplexer promise truly multiplexed bolometer arrays.

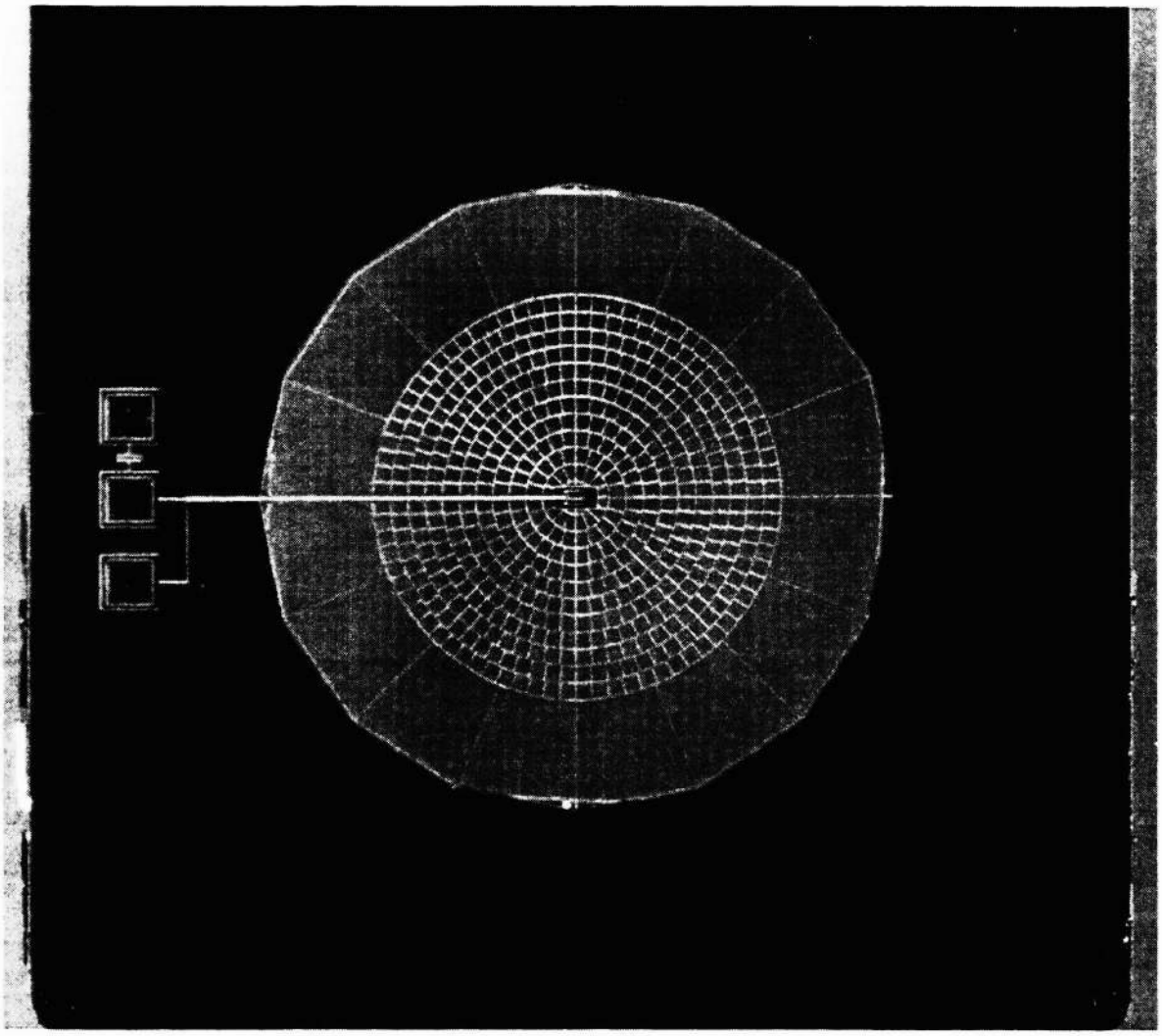

Figure 1. Silicon nitride micromesh bolometer with Ti transition-edge superconductor. Infrared radiation is absorbed in a finely patterned metalized mesh of free-standing silicon nitride thermally isolated by radial legs of bare silicon nitride. Strong electrothermal feedback maintains the superconducting film in the middle of its sharp ($d\ln(R)/d\ln(T) \sim 900$) transition with the electrical power dissipation compensating for variations in optical loading. A shunt resistor across lithographed Nb leads to the left of the device provides the voltage bias.

2. SILICON NITRIDE MICROMESH BOLOMETERS

We are developing arrays of bolometers based on an absorber made from a finely patterned mesh of silicon nitride ("spider web" bolometers). The freestanding silicon nitride structure consists of a mesh metalized for optimal absorption. The absorber is suspended by radial legs of bare silicon nitride which provide rigid mechanical support and very low thermal conductivity (see Fig. 1). The open structure of the absorber, with a geometric filling factor as low as 1.5%, maintains infrared absorption but minimizes the cosmic ray cross section and suspended mass. The resonant mechanical frequency of the bolometer ($\geq$ 25 kHz) is high due to the low suspended mass and the stiff mechanical support. The device is thus mechanically insensitive to the relatively low frequency vibrations encountered during launch and operation. Silicon nitride supports enable low thermal conductivity and therefore devices with high sensitivity. NEPs as low as 3 x 10^{-18} W/$\sqrt{}$Hz at 300 mK and 3x 10^{-19} W/$\sqrt{}$Hz at 100 mK are achievable in principle with this architecture[2].

A sensitive thermistor on the absorber detects the thermal rise due to absorbed infrared radiation. We are developing bolometers with thermistors consisting of neutron-transmutation-doped (NTD) Ge. The thermistor is attached to the absorber by indium bump bonds and is read out via evaporated Au leads lithographed onto the device. In the limit that the thermal conductance is dominated by the lithographed leads, the performance of the bolometer may be precisely controlled by the thickness of the metal film. These bolometers have reached a state of relative maturity and are the baseline detector for the Planck Surveyor. We have achieved NEPs and optical time constants of 1.2 x 10^{-17} W/$\sqrt{}$Hz and 100 ms at 300 mK[2] and 2 x 10^{-18} W/$\sqrt{}$Hz and 65 ms at 100 mK[3]. A faster time constant may be obtained at the price of larger NEP by increasing the thermal conductance G, leaving the figure of merit NEP$\sqrt{\tau}$ constant. We have developed bolometers at 100 mK with an NEP = 8 x 10^{-18} W/$\sqrt{}$Hz and an optical time constant of 4.5 ms.

For the SPIRE performance requirements, we assume 1 fλ feedhorns for the case of the photometric arrays and 2 fλ feedhorns for the spectroscopic arrays. We set the required bolometer $NEP_{Bol} = 0.5\ NEP_{Phot}$, so that the overall $NEP_{Tot} = (NEP_{Bolo}^2 + NEP_{Phot}^2)^{1/2} = 1.12\ NEP_{Phot}$. We compare the measured performance of an NTD Ge bolometer at 300 mK, with an absorber area nearly 10 times larger than required at the longest wavelength of SPIRE if used in a feedhorn-coupled arrangement, with the required performance parameters in Table 1. The bolometer meets the SPIRE requirements except in the longest wavelength spectrometer channel. We conservatively estimate that the figure of merit NEP$\sqrt{\tau}$ should decrease by at least a factor of 2 for a bolometer with the collecting area required at the SPIRE wavelengths. Even with no improvement, however, NTD Ge bolometers can meet the speed requirements and achieve $NEP_{Tot} = 1.25\ NEP_{Phot}$ at 300 mK.

We are currently developing bolometer arrays based on the silicon micromesh bolometer technology which are placed in integrating cavities located behind a close-packed array of feedhorns. The cavity-coupled arrangement is flexible and can be used in either single-mode (conical feed) or multi-mode (Winston horn) optical systems, both of which would be needed for SPIRE since the proposed FTS arrays are multi-mode. The bolometer array consists of a monolithic structure of silicon with individual detectors addressed by leads lithographed to bond pads at the edges of the wafer. The silicon wafer is placed

Table 1: Required Detector Performance for SPIRE

	Wavelength [μm]	NEP_{Phot} [x 10^{-17} W/$\sqrt{}$Hz]	τ [ms]	$NEP_{Bolo}\sqrt{\tau}$ [x 10^{-17} J]	NEP_{Tot} / NEP_{Phot}
Photometer[a]	250	8	30	0.7	1.04
	350	6	30	0.5	1.08
	500	5	30	0.4	1.12
Spectrometer[b]	200 - 300	8	10	0.4	1.12
	300 - 670	5	10	0.3	1.25
Measured Performance of NTD Ge Bolometer at 300 mK	1000 - 1800[c]	1.2	100	0.4	

[a]Specifications for 1 fλ feedhorn arrays

[b]Specifications for 2 fλ feedhorn arrays

[c]2.5 mm absorber diameter with 200 μm grid spacing.

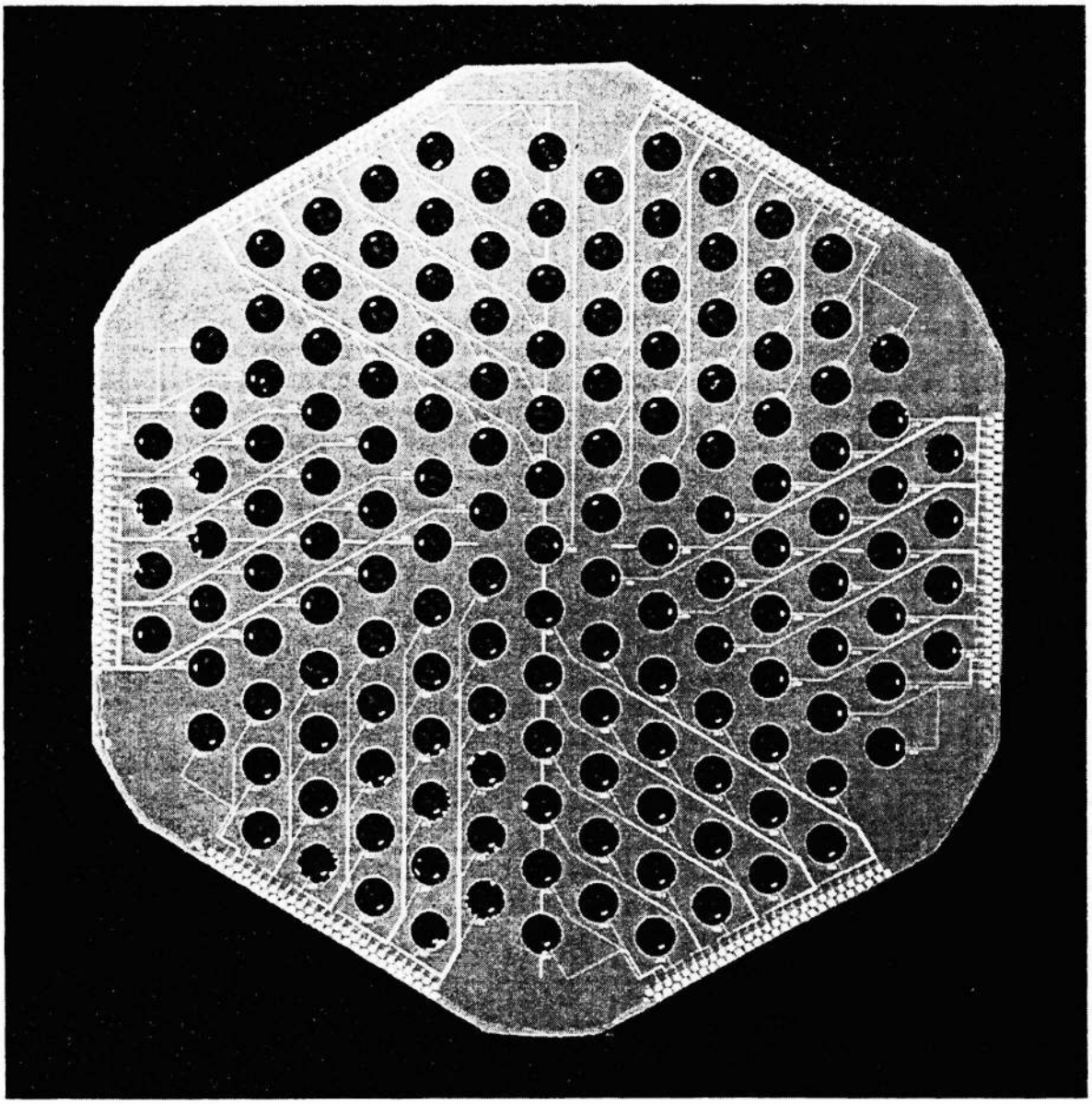

Figure 2. Large format 151 element bolometer array with NTD Ge thermistors being developed for a ground-based bolometer camera. Current fabrication methods give a membrane yield > 98 %, and further improvement can be expected with a new dry etch and release technique. The feedhorn-coupled bolometer array is readout with lithographed leads terminating in bond pads which can be easily addressed by the SQUID multiplexer.

between a close-packed array of feedhorns and an array of integrating cavities. A prototype bolometer array designed for the mm-wave camera Bolocam (see J. Glenn *et al.* in these proceedings) is shown in Fig. 2. The backup option for SPIRE consists of silicon nitride micromesh bolometers coupled to 2 fλ feedhorns and is based on the limits of current technology. We propose to improve the mapping speed of the SPIRE arrays by using feedhorns with entrance apertures smaller than 2.0 fλ, reducing the number of pointings required to make a fully sampled map, but increasing the number of detectors. We plan to demonstrate the performance of our array architecture with Bolocam.

3. FEEDHORN-COUPLED BOLOMETER ARRAYS

Bolometer arrays may be coupled to a close-packed array of conical feedhorns (e.g. SCUBA[4], bolometer array for IRAM[5]) or may be constructed in a close-packed architecture with no concentrating fore optics (e.g. SHARC[6]). It is generally known that the feedhorn arrangement with a horn diameter of 2 fλ, where f is the f-number incident on the feedhorn array, maximizes the sensitivity to a point source per detector[7]. For instruments where the number of detectors is constrained, the approach of 2 fλ feeds is therefore most appropriate. It is also generally known that in applications where the field-of-view is limited, filled arrays of detectors offer better performance than feedhorn-coupled arrays. The dominance of filled arrays at optical and infrared wavelengths, where detector array technology is well developed, demonstrates the advantage of this approach. Techniques are now emerging to make filled arrays available at submillimeter wavelengths (Moseley *et al.* in these proceedings) which may be developed in time for FIRST. The relative tradeoffs between feedhorn-coupled arrays and filled arrays, and the transition between 2 fλ feeds and feedhorn arrays with finer plate scales, are therefore important considerations in developing arrays for FIRST.

For most applications, the 2 fλ feedhorns can provide sufficient control of the detector illumination on the primary mirror so that the feedhorn views the primary directly without a cold aperture stop. FIRST, however, will have a cold aperture stop to control the illumination on the primary mirror. The cold aperture stop is necessary to control the illumination of the primary mirror with a filled bolometer array and opens the possibility of using feedhorn arrays with an opening diameter smaller than 2 fλ.

We consider the cases of d = 2 fλ, 1.4 fλ, and 1 fλ feedhorns and a filled array with 0.5 fλ pixels. The beam from each detector of the feedhorn array on the sky is approximately diffraction-limited. However, the spacing between the horns is larger than 0.5 fλ and thus requires intermediate pointings spaced by ~0.5 fλ ("jitter positions") to create a fully sampled image. First we consider the case where a pixel is centered on a point source. The incident power from the point source on the central pixel is given by

$$Q_{sig} = \eta_{opt}\, \eta_{pix}\, A\, F_\lambda\, \Delta\lambda, \tag{1}$$

where F_λ is the point source flux, A is the area of the primary mirror, η_{opt} is the optical efficiency, and η_{pix} is the pixel aperture efficiency. In the case of a filled array, the aperture efficiency is simply the enclosed fraction of the energy of the Airy function over the area of a square pixel. The background loading from thermal emission from the telescope is given by

$$Q_B = \varepsilon_{tel}\, \eta_{opt}\, A\Omega_t\, B_\lambda(T_{tel})\, \Delta\lambda, \tag{2}$$

where ε_{tel} is the emissivity of the telescope, $B_\lambda(T_{tel})$ is the blackbody function, and $A\Omega_t$ is the throughput from the detector coupling to the telescope. If the detectors are background limited, the noise is proportional to the square root of the background loading, $N = (Q_B\, h\nu\, t)^{1/2}$, where t is the integration time. The signal-to-noise ratio of the central pixel is thus given by

$$(S/N)_c = \eta_{pix}\, A\, F_\lambda\, (h\nu\, t\, \eta_{opt}\, \Delta\lambda / \varepsilon_{tel}\, A\Omega_t\, B_\lambda(T_{tel}))^{1/2} \propto \eta_{pix}\, (t\, \eta_{opt} / A\Omega_t)^{1/2}, \tag{3}$$

where we have dropped the factors relating to the telescope and wavelength which are common to all of the array options. The resulting mapping speed is proportional to

$$M_c = (S/N)_c^2 \propto \eta_{pix}^2\, (t\, \eta_{opt} / A\Omega_t). \tag{4}$$

In the case of a fully sampled map, the relative integration time of the central pixel varies inversely as the number of jitter positions = $(2d/f\lambda)^2$, ranging from 16, 8, 4, and 1 in the 2 $f\lambda$, 1.4 $f\lambda$, 1 $f\lambda$ and 0.5 $f\lambda$ cases, assuming that the overhead time involved in jittering may be neglected. The relative mapping speed of the central pixel may thus be rewritten

$$M_c \propto \eta_{pix}^2 (\eta_{opt} / A\Omega_t) (f\lambda / d)^2. \quad (5)$$

To extract the flux from a point source we must coadd the signal in the adjacent pixels out to an effective diameter of 1.5 $f\lambda$. In the case of the feedhorn arrays the nearest pixels are obtained from the jittered positions. The relative mapping speed to extract the flux from a point source is given by

$$M_{tot} = (1 + f)^2 N^{-1} \eta_{pix}^2 (\eta_{opt} / A\Omega_t) (f\lambda / d)^2, \quad (6)$$

where f is the ratio flux which falls into the neighboring pixels surrounding the central pixel compared to the flux in the central pixel, and N is the number of pixels to be coadded. The quantity N = 9 for the filled array option with square pixels

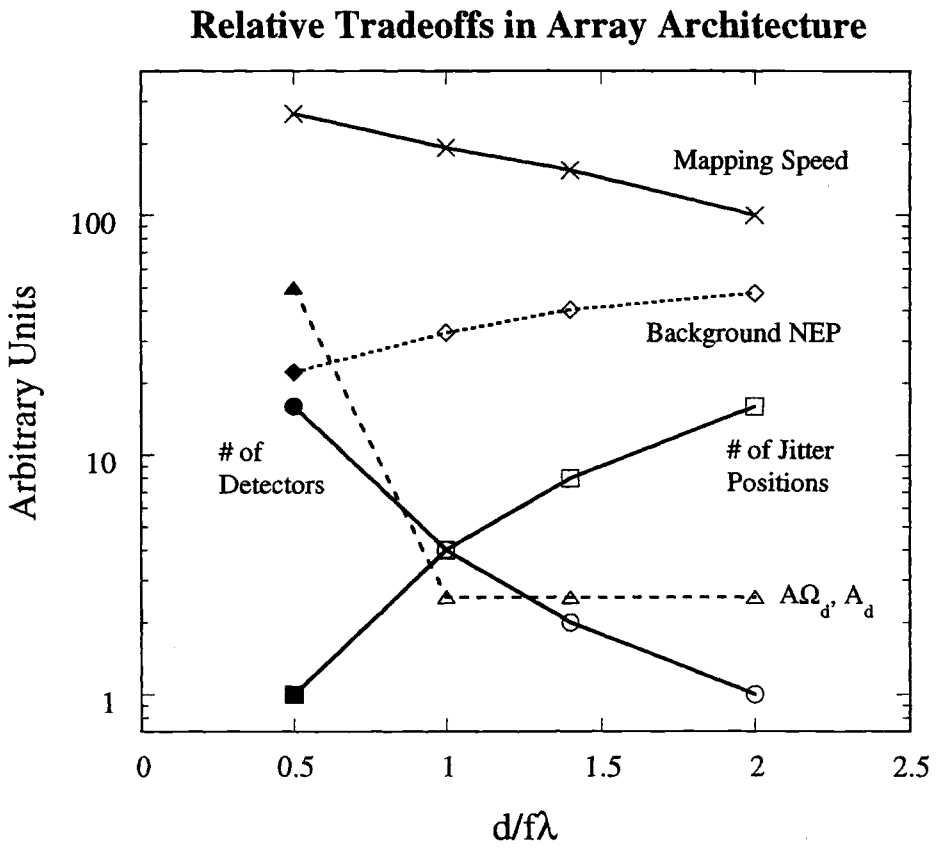

Figure 3. Relative mapping speed of array architectures with 1 $f\lambda$, 1.4 $f\lambda$, and 2 $f\lambda$ close-packed feedhorns and a 0.5 $f\lambda$ filled array operating at f / 5. The optical efficiency of the two arrays is assumed to be the same, but we note that the mapping speed scales as η_{opt} in the background limit. We also plot the NEP required to achieve background-limited performance for each detector in the array, the relative number of detectors, the number of jitter positions required to create a fully sampled image, and the relative detector throughput $A\Omega_d$ and area A_d.

and 7 for the close packed horn array options with a hexagonal pack. The relative flux $f \cong 3.5$ varies weakly between the various array options due to the slight difference in the resulting beam size on the sky. Essentially the relative mapping speed can be understood as a tradeoff between the larger detector throughput available with larger horns and the reduced integration time due to the number of jitter positions. For background-limited arrays with equivalent optical efficiency, the time required to map a region of sky to a limiting flux level is fastest for a filled array, and is longer by factors of 1.4, 1.7, and 2.6 in the case of 1 $f\lambda$, 1.4 $f\lambda$, and 2 $f\lambda$ feedhorn-coupled arrays.

Feedhorn arrays thus provide somewhat lower mapping speed than a filled array and require additional jitter positions to create a fully sampled map. However, feedhorn arrays offer several significant advantages in implementation which may ultimately outweigh the modest decrease in mapping speed. The number of detectors required to fill a given field of view is reduced, scaling as $(2d/f\lambda)^2$, reducing demand on the readout electronics and on the telemetry data rate. The detector area is minimized to $\sim\lambda^2/\pi$ for feedhorn-coupled arrays, compared to $\sim f^2\lambda^2/4$ for filled arrays, minimizing cosmic ray cross-section and suspended mass. The throughput of each detector is λ^2 for feedhorn-coupled arrays, compared to $\pi f^2\lambda^2/4$ for filled arrays, reducing the response to stray radiation from the instrument. Because the detector throughput to the telescope is larger for a feedhorn coupled bolometer, the required NEP to achieve background-limited sensitivity is larger, scaling as $NEP_B = (\eta_{opt} A\Omega_t)^{1/2}$. The relative tradeoffs between a filled array with 0.5 $f\lambda$ pixels, assuming f = 5, and 1.0 $f\lambda$, 1.4 $f\lambda$, and 2.0 $f\lambda$ feedhorn arrays are shown graphically in Fig. 3. Feedhorn arrays with even smaller pixels (0.5 $f\lambda$) are possible, and because η_{pix} and $A\Omega_t$ approach the values for bare pixels, they have similar mapping speed compared with filled arrays.

Feedhorn-coupled bolometers currently demonstrate high optical efficiency. A mm-wave feedhorn structure has been constructed with a total measured optical efficiency of 40 % including the absorption in a micromesh bolometer and bandpass and low-pass filtering with excellent high frequency rejection[8]. Feedhorn arrays may also be used to form one wall of an RF-tight box surrounding the bolometers and low-temperature amplifiers, minimizing susceptibility to electromagnetic interference. Finally, many of the SPIRE observations will be of unresolved sources with known position. For example, protogalaxy candidates detected by the far-infrared and submillimeter cameras will be natural targets for spectroscopic study with the imaging FTS. In this case, the $2f\lambda$ feedhorn array without jitter positions offers higher sensitivity, giving a speed advantage of 1.4 relative to the 0.5 $f\lambda$ filled array option with optimal weighting for flux extraction, and 1.7 and 1.1 relative to the 1.0 $f\lambda$ and 1.4 $f\lambda$ feedhorn array options, respectively.

New array architectures and low-temperature multiplexers may soon resolve the significant technical challenges posed by filled arrays: optical efficiency, straylight susceptibility, detector size, low-temperature readout, and data rate. Feedhorn-coupled bolometer arrays offer comparable ultimate performance while greatly relaxing the technical demands, and provide a continuum of options between 2 $f\lambda$ feedhorn arrays and filled arrays.

4. TRANSITION-EDGE BOLOMETERS

Although NTD Ge bolometers can give the individual device performance required by the SPIRE bolometer arrays, the current readout technology of one cold Si JFET, one warm amplifier, and one wire from ambient temperature to 300 mK per detector, limits the array format for SPIRE to 2 $f\lambda$ feedhorns due to limits on the power dissipation at the focal plane. Semiconducting bolometers could be multiplexed with a single JFET amplifier and a cold low-power switch at 300 mK. However, the number of detectors per amplifier is constrained by the RC time constant of the bolometer, the circuit capacitance, and the comparatively large voltage noise of a Si JFET. With power dissipation of order ~1 mW per JFET, even a multiplexed JFET read out still dissipates significant power at the focal plane.

Transition-edge superconductors[9] can be used instead of NTD Ge, providing additional performance due to the steepness of the transition ($d\ln(R)/d\ln(T) \sim 1000$ measured for Ti films compared to $d\ln(R)/d\ln(T) \sim 5$ for NTD Ge). The film is voltage-biased at the center of the transition. Electrothermal feedback, of secondary importance with semiconducting thermistors but dominant with the voltage-biased TES, maintains the device at the center of the transition with the electrical power varying to compensate for changes in the optical loading. Electrothermal feedback reduces Johnson noise by 2 orders of magnitude at low frequencies so that the noise is dominated by phonon noise, surpressing low frequency noise in the superconducting film. The speed of response of the bolometer increases by

$$\tau = (C/G)\,(1 + P_b A/GT)^{-1} \sim (C/G)\,(10/A), \qquad (7)$$

where A = dln(R)/dln(T) can be on order of 1000. For bolometers with micromesh absorbers the speed of response will eventually be limited by the internal thermalization time of the absorber, which is estimated to be of order 1 ms[10].

Although TES bolometers offer improved performance with a better figure of merit NEP$\sqrt{\tau}$, of more importance for SPIRE are the advantages of the readout. Voltage-biased transition-edge bolometers may be readout with a SQUID current amplifier. The dissipation of a SQUID amplifier, of order ~nW compared to the ~mW power dissipation of a JFET, allows the cold amplifier to be placed directly on the 300 mK stage. A SQUID-based multiplexer being developed at the National Institute of Standards and Technology promises truly multiplexed arrays of bolometers with relatively few leads from the 300 mK stage. The multiplexer incorporates a first stage SQUID amplifier array, with one SQUID per device. A second stage series SQUID addresses individual elements in a column of the array by switching the bias lines of the first stage SQUID amplifier, reading each detector sequentially. The cold multiplexer is a critical technology for SPIRE since it enables the larger format 1 fλ feedhorn-coupled or 0.5 fλ filled array options.

5. CONCLUSIONS

We are developing a multiplexed bolometer array for SPIRE with 1 fλ feedhorns. An ideal 1 fλ array offers 0.7 the mapping speed compared to an ideal filled array, but has the advantages of minimal detector area and throughput and high optical efficiency. The optical performance of the array will be demonstrated with the ground-based bolometer camera Bolocam. Voltage-biased TES bolometers and a SQUID multiplexer promise the large format, truly multiplexed 2-D arrays needed to enhance the performance of SPIRE.

6. ACKNOWLEDGMENTS

We would like to thank Matt Griffin and Walter Gear their contributions in the calculation of the mapping speed for the array architectures. The authors acknowledge support from NASA Innovative Research Grant NAG5-3465 and the Advanced Technology Program at JPL.

7. REFERENCES

1. Puget, J.L., Abergel, A., Bernard, J.P., Boulanger, F., Burton, W.B., Desert, F.-X., and Hartmann, D., "Tentative Detection of a Cosmic Far-Infrared Background with COBE," *Astron. and Astrop.*, **308,** pp. L5-L8.
2. Bock, J.J., DelCastillo, H.M., Turner, A.D., Beeman, J.W., Lange, A.E., and Mauskopf, P.D., "Infrared Bolometers with Silicon Nitride Micromesh Absorbers," *Proc. 30th ESLAB Symp. ESA SP-388*, pp. 119-122, 1996.
3. Murray, A.G., Ade, P.A.R., Bhatia, R.S., Griffin, M.J., Maffei, B., Nartallo, R., Beeman, J.W., Bock, J., Lange, A., and DelCastillo, H., "Testing of 100 mK Bolometers for Space Applications," *Proc. 30th ESLAB Symp. ESA SP-388*, pp. 127-130, 1996.
4. Cunningham, C.R., Gear, W.K., Duncan, W.D., Hastings, P.R., and Holland, W.S., "SCUBA: The Submillimeter Common-User Bolometer Array for the James Clerk Maxwell Telescope," *Proc. SPIE Symp. on Instrumentation in Astronomy VIII*, **2198,** pp. 638-649, 1994.
5. Kreysa, E., Beeman, J.W., and Haller, E.E., "Micromachined Bolometer Arrays with Silicon-Nitride Membranes," *Proc. 30th ESLAB Symp. ESA SP-388*, pp. 111-114, 1996.
6. Wang, N., Hunter, T.R., Benford, D.J., Serabyn, E., Phillips, T.G., Moseley, S.H., Boyce, K., Szymkowiak, A., Allen, C., Mott, B., and Gygax, J., "Characterization of a submillimeter high-angular-resolution camera with a monolithic silicon bolometer array for the Caltech Submillimeter Observatory," *Appl. Opt.*, **35,** pp. 6629-6640, 1996.
7. Gear, W.K., and Cunningham, C.R., "SCUBA: a submillimeter camera," *Proc. 29th Liege Colloquium, From Ground-Based to Spaceborne Sub-mm Astronomy ESA SP-314*, pp. 353-358, 1990.
8. Church, S.E., Philhour, B., Lange, A.E., Ade, P.A.R., Maffei, B., Nartallo-Garcia, R., and Dragovan, M., "A Compact High-Efficiency Feed Structure for Cosmic Microwave Background Astronomy at Millimeter Wavelengths," *Proc. 30th ESLAB Symp. ESA SP-388*, pp. 77-80, 1996.
9. Lee, A.T., Richards, P.L., Nam, S.W., Cabrera, B., and Irwin, K.D., "A Superconducting Bolometer with Strong Electrothermal Feedback," *Appl. Phys. Lett.*, **69,** pp. 1801-1803, 1996.
10. Bock, J.J., Chen, D., Mauskopf, P.D., and Lange, A.E., "A Novel Bolometer for Infrared and Millimeter-wave Astrophysics," *Space Science Reviews*, **74,** 229-235, 1995.